Bifurcation of Pulsation Instability in One-Dimensional H_2-O_2 Detonation with Detailed Reaction Mechanism

Wenhu Han[1, 2, *], Wenjin Ma[1], Chengeng Qian[1], Jennifer Wen[2], Cheng Wang[1, *]

[1]*State Key Laboratory of Explosion Science and Technology, Beijing Institute of Technology, Beijing 100081, China*

[2] *School of Engineering, University of Warwick, Coventry, CV4 7AL, UK*

**Corresponding author: Email: hanwenhu@bit.edu.cn; wangcheng@bit.edu.cn*

Abstract: Classical modes of one-dimensional (1-D) detonation characterized by simplified reaction model are reproduced through by using a real chemical kinetics for the H_2-O_2 system with argon dilution. As varied Ar dilution, the bifurcation points of pulsating instability are identified and a formed bifurcation diagram is compared with that obtained by the one-step reaction model. Eventually, the numerical results demonstrate that for real detonations with detailed chemistry, the criterion of Ng. et al. works well on prediction of the 1-D detonation instability. Furthermore, the detonability limits are found respectively at low and high Ar dilutions. Above the high Ar dilution limit, detonations decays to the minimum level where long autoignition time and small heat release rate make re-establishment impossible for both 1-D and 2-D simulations. However, below the low Ar dilution limit, a 1-D detonation cannot be sustained due to highly instability, while the corresponding cellular detonation can propagate sustainingly due to the role of transverse instability.

Keyword: detonation, pulsation, detailed reaction, diffusion

1. Introduction

A detonation wave manifested pulsations in one dimension [1] and cellular instability in multiple dimensions [2-5], depending on the initial conditions and mixture properties. For pulsating detonation near Chapman-Jouguet (C-J) state, extensive

experiments and theoretical analyses have observed longitudinal oscillation of the detonation front [6-11]. Specially, the theoretical studies of Clavin & Williams [2,3,12] has milestone significance for the physical explanation of origin of 1-D instability and the relation of pulsating and cellular instabilities. He & Lee [13] examined the 1-D instability of detonation and demonstrated that 1-D detonations in the planar geometry are classified into three classes through identifying the boundary of detonation stability, and observed different modes of shock oscillation: neutral stability, pulsation with a single-mode oscillation and with multi-period mode, and highly nonlinear and even chaotic oscillations. Sharpe & Falle [14] observed a series of failures followed by re-ignition for a highly unstable detonation with a large activation energy and found the cause of instabilities in reaction zone by using a one-step overall reaction. Romick, Aslam & Powers [15] studied the effect of diffusion on the dynamics of unsteady detonations with a one-step overall reaction, and found that diffusion influenced strongly the dynamics of unstable detonation. Ng *et al*. [16] examined the study of 1-D detonation using a two-step reaction model and proposed a universal criterion for 1-D detonation instability by defining a stability factor, and given bifurcation diagram of pulsating detonation. A three-step chain-branching reaction model was used to predict detonability limit by Short & Quirk [17]. As the studies of chemical reaction kinetics are advanced, realistic chemistry is used to calculate the stability of 1-D detonations. Radulescu *et al*. [18] used a seven-step chemistry model to simulate 1-D detonation propagation in acetylene/oxygen mixture and investigated the effect of argon dilution in stabilizing detonations. Yungster & Radhakrishnan [19] investigated the high-

frequency and small-amplitude pulsation for overdriven detonations supported by a piston and revealed the effect of initial pressure on pulsating mode. Romick, Aslam & Powers [20] used detailed H_2-air mechanism to establish a bifurcation diagram of peak shock pressure with the change in overdriven factor determined by a piston velocity through calculation of the 1-D viscous detonation with a supporting piston [21, 22]. Sussman [23] simulated pulsating detonations by using a detailed H_2/air mechanism, concluding that the pulsating propagation depends on the ratio of heat release time to induction time. In general, however, the studies of 1-D detonations with real chemistry have been few for pulsating instability of detonations globally close to CJ state.

The present work aims to examine the propagation mode of 1-D detonation driven by real chemistry and to give pulsation bifurcation diagram for H_2-O_2-Ar system. In the following we shall first state the governing equations and the numerical method, and then present and discuss the results.

2. Governing equations

The governing equations are the one-dimensional, reactive, compressible N-S equations:

$$\frac{\partial \rho}{\partial t}+\frac{\partial \rho u}{\partial x}=0 \tag{1}$$

$$\frac{\partial \rho u}{\partial t}+\frac{\partial (\rho u^2+p\text{-}\tau)}{\partial x}=0 \tag{2}$$

$$\frac{\partial \rho uE}{\partial t}+\frac{\partial \rho uE+(p\text{-}\tau)u+q}{\partial x}=0 \tag{3}$$

$$\frac{\partial \rho Y_i}{\partial t}+\frac{\partial \rho uY_i+\zeta_i}{\partial x}=\bar{W}_i\dot{\omega}_i,\ i=1,\ \ldots\ ,\ N\text{-}1 \tag{4}$$

$$E=h+\frac{p}{\rho}+\frac{u^2}{2} \tag{5}$$

$$p = \sum_{i=1}^{N} \rho Y_i R_i T = \rho \left(\sum_{i=1}^{N} Y_i R_i \right) T \quad , \quad R_i = \frac{R_u}{\bar{W}_i} \tag{6}$$

$$h = \sum_{i=1}^{N} Y_i h_i \, , \tag{7}$$

$$h_i(T) = h_i^f + \int_{T_0}^{T} c_{p,i}(\hat{T}) d\hat{T} \, , \tag{8}$$

where p, ρ, E, T, u, h are the pressure, the density, the total energy per unit mass, the temperature, the x- velocities and the enthalpy per unit mass; Y_1, …, Y_N is the mass fraction of ith species, with $\sum_{i=1}^{N} Y_i = 1$; W_i, R_i, c_{pi} and h_i^f are the molecular weight, the specific gas constant, the specific heat and the enthalpy of formation of ith species, and R_u = 8.31 J/(mol K) the universal gas constant. To close the system, constitutive relations are specified for an ideal mixture of N species,

$$\tau = \frac{4\mu \partial u}{3 \partial x} \tag{9}$$

$$\zeta_i = -\frac{D_i^T \partial T}{T \partial x} + \rho \sum_{\substack{k=1 \\ k \neq i}}^{N} \frac{\bar{W}_i D_{ik} X_k}{\bar{W}} \left(\frac{1}{X_k} \frac{\partial X_k}{\partial x} \right) + \left(1 - \frac{\bar{W}_k}{\bar{W}}\right) \frac{1}{p} \frac{\partial p}{\partial x} \tag{10}$$

$$q = -\kappa \frac{\partial T}{\partial x} + \sum_{i=1}^{N} \zeta_i h_i - R_u T \sum_{i=1}^{N} \frac{D_i^T}{\bar{W}_i} \left(\frac{1}{X_i} \frac{\partial X_i}{\partial x} + \left(1 - \frac{\bar{W}_i}{\bar{W}}\right) \frac{1}{p} \frac{\partial p}{\partial x} \right) \tag{11}$$

$$X_i = \frac{\bar{W}}{\bar{W}_i} Y_i \tag{12}$$

$$\bar{W} = \left(\sum_{i=1}^{N} \frac{Y_i}{\bar{W}_i} \right)^{-1} \tag{13}$$

where $\bar{W}$ is the mixture molecular mass, D_{ik} the multi-component diffusion coefficient between the ith and kth species, D_i^T the thermal diffusion coefficient of the ith species, T the temperature, μ the dynamic viscosity of the mixture, κ the thermal conductivity of the mixture, and $X_1 \ldots X_N$ are the mole fractions of species i, with $\sum_{i=1}^{N} X_i = 1$. The mixture properties are evaluated using the CHEMKIN [24] and TRANSPORT [25] packages. We adopt the San Diego mechanism [26] which

comprises the eight species H_2, O_2, OH, O, H, H_2O, HO_2 and H_2O_2.

3. Numerical method

The semi-discretization of governing equations (1-4) is as follows,

$$\frac{\mathrm{d}U}{\mathrm{d}t}=H_a(U)+H_d(U)+H_s(U) \tag{14}$$

where $H_a(U)$, $H_d(U)$ and $H_s(U)$ are approximations of advection term, diffusion term and reaction source term, respectively. The numerical flux $\hat{F}_{a,i+1/2}$ in the advection term $H_a(U)=-\dfrac{\hat{F}_{a,i+1/2}+\hat{F}_{a,i-1/2}}{\Delta x}$ is obtained with fifth order WENO reconstruction [27] as presented in the following. The physical flux $\boldsymbol{F}_a$ can be divided by using Lax-Friedrichs flux splitting,

$$\boldsymbol{F}_a^{\pm}=\frac{1}{2}(F_a\pm\alpha U) \tag{15}$$

where $\alpha=\max|\lambda|$ and λ are the eigenvalues of Jacobian Matrix for $\boldsymbol{F}_a$.

For simplicity, we only present the reconstruction of numerical flux $\hat{\boldsymbol{F}}^{+}_{a,i+1/2}$ which is an approximation of $\boldsymbol{F}^{+}_{a,i+1/2}$. The fifth order numerical flux is given by

$$\hat{\boldsymbol{F}}^{+}_{a,i+1/2}=\sum_{r=0}^{2}\omega_r F^{+,(r)}_{a,i+1/2}\ . \tag{16}$$

where the third order numerical fluxes on three small stencils are given by

$$\hat{\boldsymbol{F}}^{+,(1)}_{a,i+1/2}=\frac{1}{3}F^{+}_{i-2}-\frac{7}{6}F^{+}_{i-1}+\frac{11}{6}F^{+}_{i} \tag{17}$$

$$\hat{\boldsymbol{F}}^{+,(2)}_{a,i+1/2}=-\frac{1}{6}F^{+}_{i-1}+\frac{5}{6}F^{+}_{i}+\frac{1}{3}F^{+}_{i+1} \tag{18}$$

$$\hat{\boldsymbol{F}}^{+,(3)}_{a,i+1/2}=\frac{1}{3}F^{+}_{i}+\frac{5}{6}F^{+}_{i+1}-\frac{1}{6}F^{+}_{i+2} \tag{19}$$

and the nonlinear weights ω_r are defined as

$$\omega_r=\frac{\alpha_r}{\sum_{s=0}^{2}\alpha_s},\alpha_r=\frac{d_r}{(\varepsilon+\beta_r)^2} \tag{20}$$

Here the linear weights d_r are given by

$$d_1=\frac{1}{10},\ \ d_2=\frac{3}{5},\ \ d_3=\frac{3}{10}$$

and the smoothness indicators β_r are given by

$$\beta_r=\frac{13}{12}(F_{i-2}^{+}-2F_{i-1}^{+}+F_i^{+})^2+\frac{3}{12}(F_{i-2}^{+}-2F_{i-1}^{+}+F_i^{+})^2 \tag{21}$$

$$\beta_2=\frac{13}{12}(F_{i-1}^{+}-2F_i^{+}+F_{i+1}^{+})^2+\frac{3}{12}(F_{i-1}^{+}-F_{i+1}^{+})^2 \tag{22}$$

$$\beta_2=\frac{13}{12}(F_i^{+}-2F_{i+1}^{+}+F_{i+2}^{+})^2+\frac{3}{12}(3F_i^{+}-4F_{i+1}^{+}+F_{i+2}^{+})^2 \tag{23}$$

The parameter ε=10^{-6} is to ensure that the denominator is not zero. Diffusion term H_d is discretized by the 6$^{\text{th}}$-order central difference scheme.

To solve the stiffness problem, an explicit-implicit additive Runge-Kutta scheme [28] was used in the time discretization. The equation (14) is written as,

$$\begin{cases}\dfrac{d\boldsymbol{U}}{dt}=\boldsymbol{H}_{ns}(\boldsymbol{U})+\boldsymbol{H}_s(\boldsymbol{U})\\ \boldsymbol{H}_{ns}(\boldsymbol{U})=\boldsymbol{H}_a(\boldsymbol{U})+\boldsymbol{H}_d(\boldsymbol{U})\end{cases}. \tag{24}$$

Additive Runge-Kutta scheme is used mainly to separate the stiff term $\boldsymbol{H}_s(\boldsymbol{U})$ and non-stiff term $\boldsymbol{H}_{ns}(\boldsymbol{U})$. The Explicit Runge-Kutta (ERK) scheme is utilized to integrate $\boldsymbol{H}_{ns}(\boldsymbol{U})$, while $\boldsymbol{H}_s(\boldsymbol{U})$ is handled by Explicit Singly Diagonally Implicit Runge-Kutta (ESDIRK) scheme.

$$\begin{cases}\boldsymbol{U}^{(i)}=\boldsymbol{U}^{(n)}+\boldsymbol{X}^{(\mathrm{i})}+(\Delta t)a_{ii}^{[I]}\boldsymbol{H}_s^{(i)},\ \boldsymbol{X}^{(\mathrm{i})}=(\Delta t)\sum_{j=1}^{i-1}\left(a_{ij}^{[E]}\boldsymbol{H}_{ns}^{(j)}+a_{ij}^{[I]}\boldsymbol{H}_s^{(j)}\right),\ i=2,\cdots,s+1\\ \boldsymbol{U}^{(n+1)}=\boldsymbol{U}^{(n)}+(\Delta t)\sum_{j=1}^{s}\left(b_j^{[E]}\boldsymbol{H}_{ns}^{(j)}+b_j^{[I]}\boldsymbol{H}_s^{(j)}\right)\end{cases} \tag{25}$$

where Δt is the time step size; $\boldsymbol{U}^{(n)}$ is the initial physical value; $\boldsymbol{U}^{(i)}$ is the intermediate physical value; $\boldsymbol{U}^{(n+1)}$ is the final physical value; $a_{ij}^{[E]}$, $a_{ij}^{[I]}$, $b_j^{[E]}$ and $b_j^{[I]}$ are the Butcher coefficients, which are constrained by some accuracy and stability considerations; $\boldsymbol{X}^{(\mathrm{i})}$ is calculated with the given data $\boldsymbol{U}^{(n)}$ explicitly; $\boldsymbol{H}_s^{(i)}$ and $\boldsymbol{U}^{(i)}$ are calculated by implicit method for solving nonlinear equations

with Newton iteration. The first term of form (11) is developed into

$$\begin{cases} \boldsymbol{M}\boldsymbol{d}_k^{(i)} = \boldsymbol{r}_k^{(i)} \\ \boldsymbol{M} = \left(\boldsymbol{I} - (\Delta t)\, a_{ii}^{[I]} \left. \dfrac{\partial \boldsymbol{H}_s}{\partial \boldsymbol{U}} \right|_k \right) \\ \boldsymbol{d}_k^{(i)} = \left(\boldsymbol{U}^{(i)} - \boldsymbol{U}_k^{(i)} \right) \\ \boldsymbol{r}_k^{(i)} = -\left(\boldsymbol{U}_k^{(i)} - \boldsymbol{U}^{(n)} \right) + \boldsymbol{X}^{(\mathrm{i})} + (\Delta t)\, a_{ii}^{[I]} \boldsymbol{H}_s^{(i)} \left(\boldsymbol{U}_k^{(i)} \right) \end{cases} \tag{26}$$

where subscript k is variable value of the k-th iteration; $\boldsymbol{M}$ is the iterative matrix; $\boldsymbol{d}_k^{(i)}$ is the difference between the iterative and real value; $\boldsymbol{r}_k^{(i)}$ is the remainder value of the iteration equation; when $\left|\boldsymbol{d}_k^{(i)}\right| \le \varepsilon$ or $\left|\boldsymbol{r}_k^{(i)}\right| \le \varepsilon$, the iteration terminates. The iteration value $\boldsymbol{U}_k^{(i)}$ can be used as $\boldsymbol{U}^{(i)}$, and thereby $\boldsymbol{H}_s^{(i)}$ is calculated with $\boldsymbol{U}^{(i)}$, finally physical value $\boldsymbol{U}^{(n+1)}$ is calculated by the terms of form (11) with $\boldsymbol{H}_s^{(i)}$ and $\boldsymbol{H}_{ns}^{(i)}$.

The CFL number is 0.2 in the simulations. Eventually, the method based on conservation variables was used to solve the equations, which guarantees conservation and also yields good solution with the shock speed evaluated accurately [29].

3. Results and discussions

3.1 Numerical specifications

The mixture has constant initial pressure and temperature of p_0=1atm and T_0=298K, respectively. Induction length is defined as the distance from the shock front to the maximum thermicity, while reaction zone is the length between peak thermicity and the reaction equilibrium. With argon dilution, the change of post-shock temperature, T_{VN} is small with the bounds of 1920 K < T_{VN} < 2050 K for 15% -85%, while it is ~1491K for 90%Ar. The corresponding C-J detonation velocity D_{CJ}, the ignition delay

time τ, the reaction length l_R and the induction length l_i as functions of Ar dilution are calculated by Cantera, as shown in Fig. 1.

The steady ZND solution including species information is set as the initial condition in the unsteady 1-D simulation and the resulting detonation is allowed to propagate into the mixture at rest to observe the long-time behavior of the detonation propagation. As the overdriven detonation is close to the CJ state, boundary conditions at the piston are then replaced by the condition at the downstream end of the reaction zone, where there is no acoustic wave propagation in the burnt gas directed upstream towards the reaction zone [12]. For freely propagating detonations, disturbance at rear boundary always is reflected in the laboratory frame. Although it is usually assumed that its influence is small, it is not confirmed whether it changes the dynamics of detonation. To avoid the influence, rear boundary in the downstream is placed at x = -0.01m and is enough far away from the detonation front so that the solution is not affected by the disturbance from the rear boundary. The value at the C-J state with flow and chemical equilibriums is fixed at the rear boundary. The computational domain is 0.12m and the grid resolution is 60pts/$l_{1/2}$, where $l_{1/2}$ is half of reaction length, l_R, and corresponds to each Ar dilution, as shown in Fig. 1. The numerical scheme reaches 5th order at smooth region [29] and hence the grid resolution of 60pts/$l_{1/2}$ is sufficient to capture detonation structures.

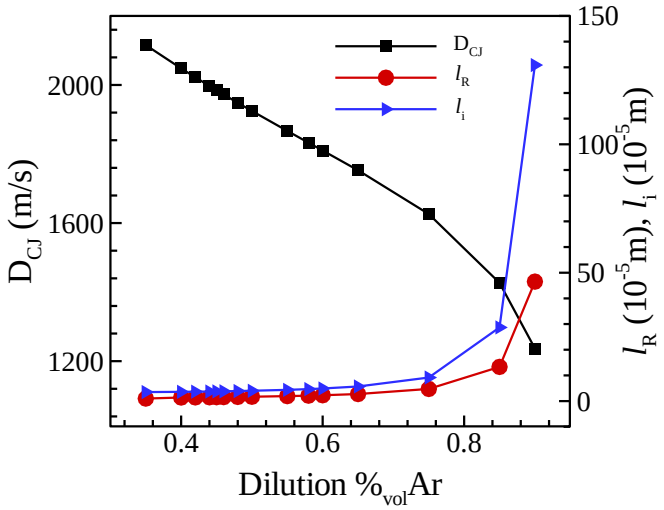

Fig. 1 Induction length, reaction length and C-J velocity for H_2-O_2 detonations with different argon dilutions at T_0=298K and p_0=1atm.

We assess the effect of diffusion on the 1-D detonation pulsation. Figure 2 shows the maximum pressure histories of detonations with the NS and Euler for 35%Ar and 50%Ar, respectively. It is seen that for 35%Ar, detonation takes on highly unstable mode, and the pulsations obtained with the NS and Euler have obvious differences in the amplitude of oscillations, indicating that diffusion has obvious effect on the chaotic characteristics. The viscous detonation has smaller amplitude of oscillations than that solved by Euler, which agrees with the findings of Romick, Aslam & Powers [30]. For 50%Ar, both the NS and Euler show almost uniform evolution of single-period pulsation, with small disparity appearing just at peaks of the pulsation. Consequently, this indicates that diffusion plays a role in an unstable detonation, while the influence is minor for the detonation with a single-period mode. Generally, viscosity is minor for a global CJ detonation. Nevertheless, we still use reactive flow NS in the following simulations.

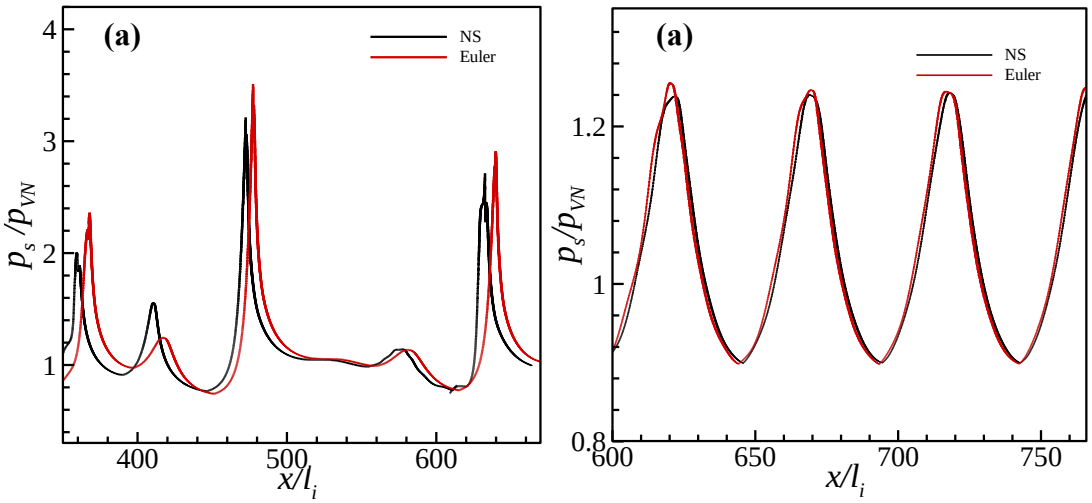

Fig. 2 Maximum pressure histories of 1-D detonations with and without diffusion for 35%Ar (a) and 50%Ar (b): p_{VN} is the steady von-Neumann value and p_s is shock pressure.

From Fig. 3, the detonations with 60 and 120 pts/$l_{1/2}$ are consistent for 35%Ar, with minor difference at the peaks of oscillations. This demonstrates that the present grid resolution is enough to capture the detonation structure. In the statement, the numerical scheme can reach 5th order when a smooth initial solution assumed, while it goes back to 1st order at the discontinuity. In fact, for all numerical schemes to treat strong discontinuity, its order drops to the 1st order.

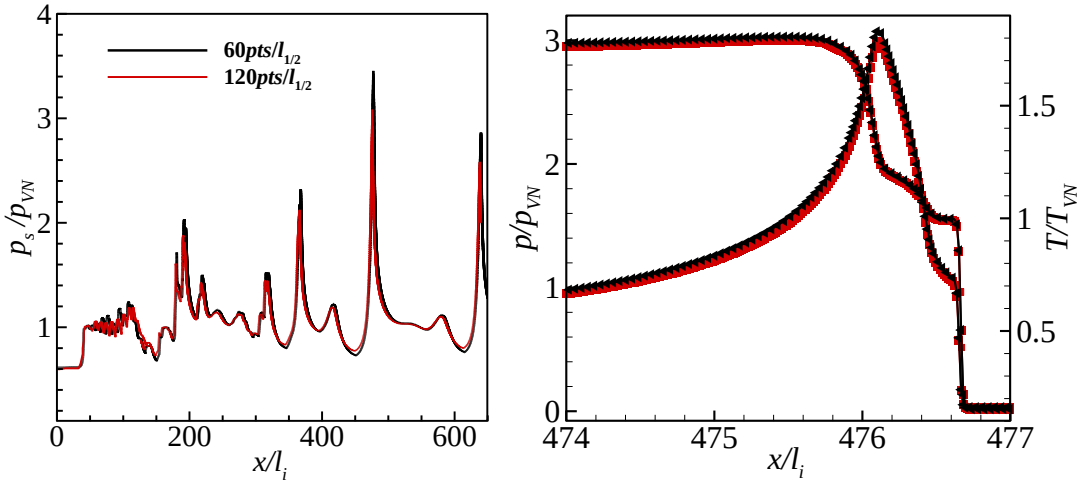

Fig. 3 Maximum pressure histories and detonation structure with 60 and 120 pts/$l_{1/2}$ for 35%Ar.

3.2 Propagation modes of 1-D detonations for different Ar dilutions

Figure 4 shows typical modes of 1-D detonations for different Ar dilutions. It is seen that the high-frequency pulsation appearing in the initial stage oscillates globally and then develops into different propagation modes for the different cases. It is seen that the detonation fails to sustaining after several high-frequency oscillations for 15%Ar dilution. As the dilution increases, pulsation shifts from the chaotic mode to stable mode. From 35% to 40%Ar dilution, detonation pulsations are chaotic, as shown in Fig. 4(b-d). From 44% to 48%Ar dilutions, multi-period modes are eventually formed; as Ar dilution increases, the minimum peak increases while the maximum peak decreases shown in Fig. 4(e-g), showing that the pulsation tends to be regular. Single-period modes appear in the cases with 50%-58%Ar dilutions, shown in Fig. 4(h-j). For 65%-85%Ar dilutions, detonations tend to be stable after several small pulsations, as shown in Fig. 4(k-l). As 90%Ar, initially established detonation decays and quenches after a strong pressure pulse, showing that detonability limit is reached and a sustaining propagation is not formed due to low heat release rate for the large dilution.

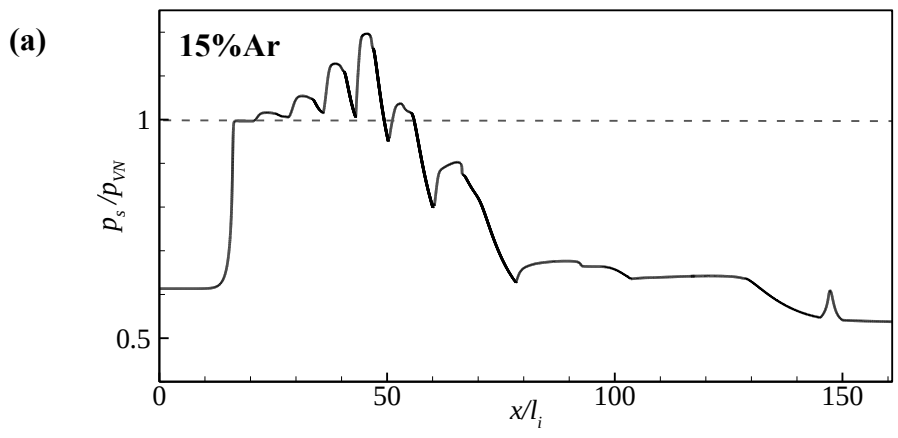

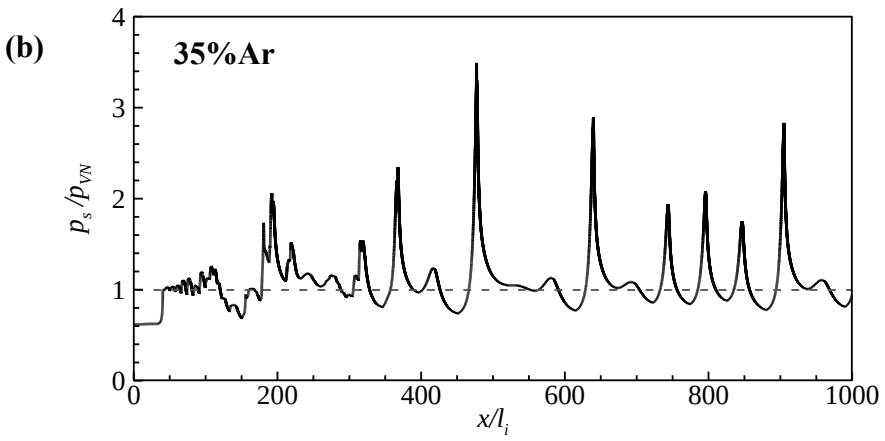
(b)
35%Ar
p_s/p_{VN}
x/l_i

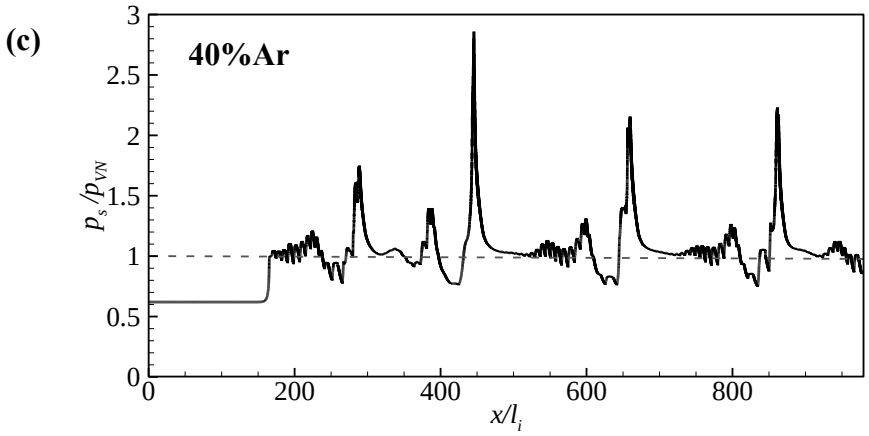
(c)
40%Ar
p_s/p_{VN}
x/l_i

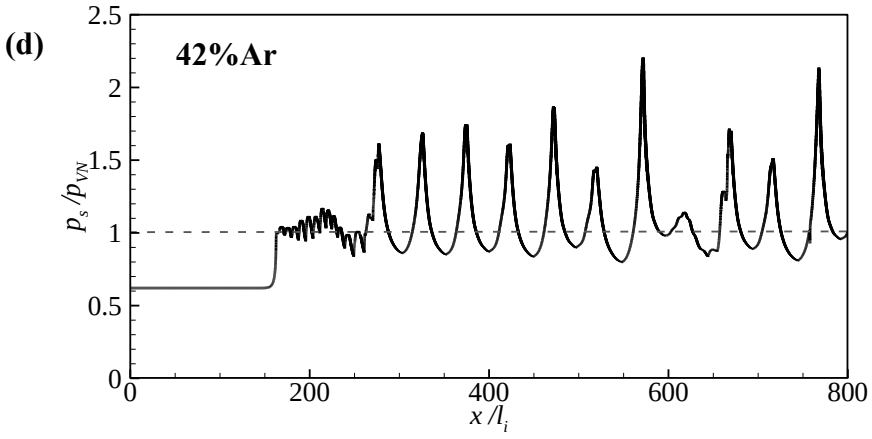
(d)
42%Ar
p_s/p_{VN}
x/l_i

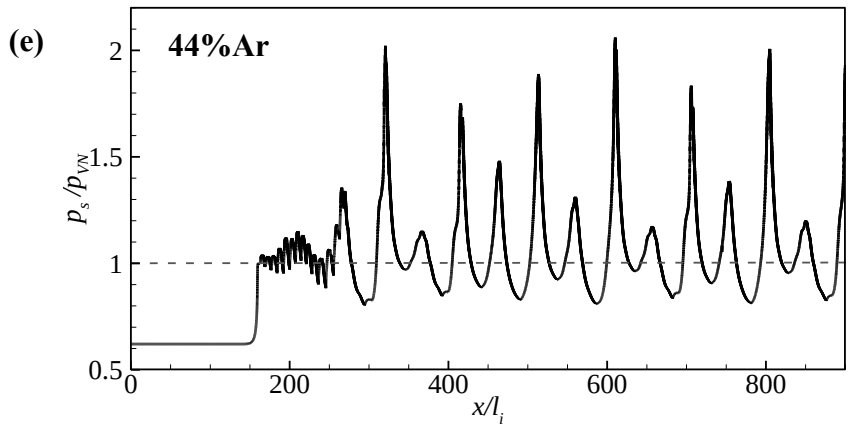
(e)
44%Ar
p_s/p_{VN}
x/l_i

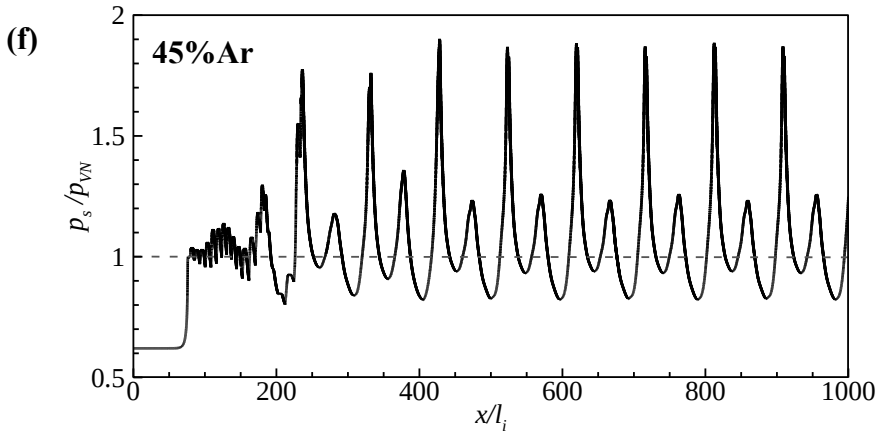
(f)
45%Ar
p_s/p_{VN}
x/l_i

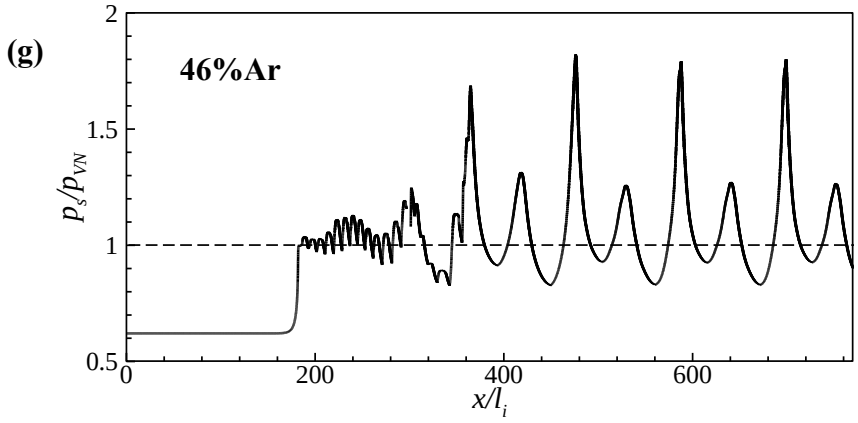
(g)
46%Ar
p_s/p_{VN}
x/l_i

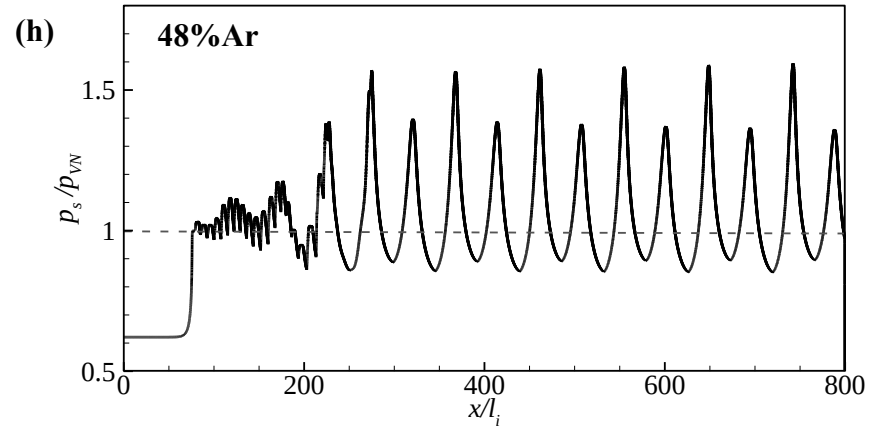
(h)
48%Ar
p_s/p_{VN}
x/l_i

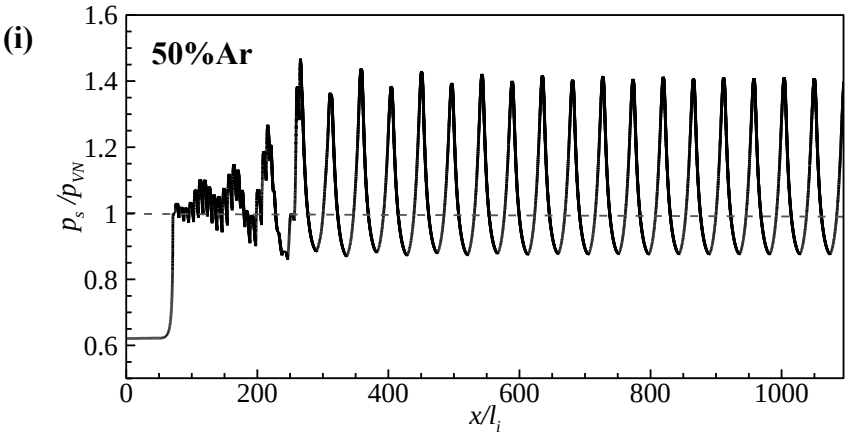
(i)
50%Ar
p_s/p_{VN}
x/l_i

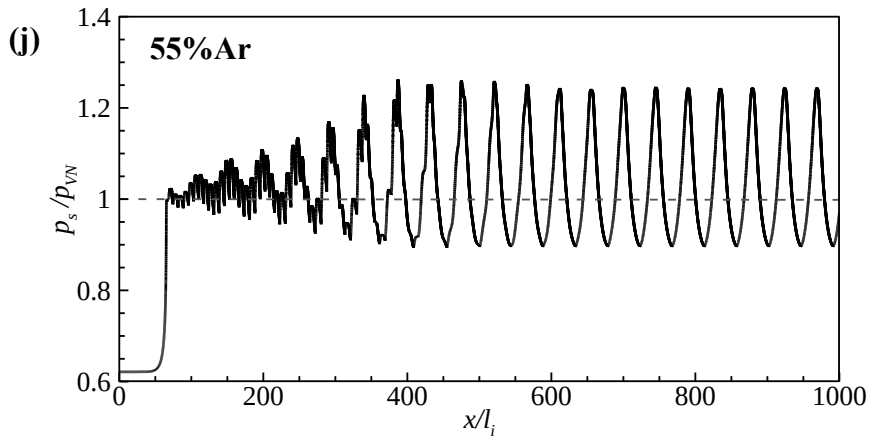
(j)
55%Ar
1.4
1.2
1
0.8
0.6
p_s/p_{VN}
0
200
400
600
800
1000
x/l_i

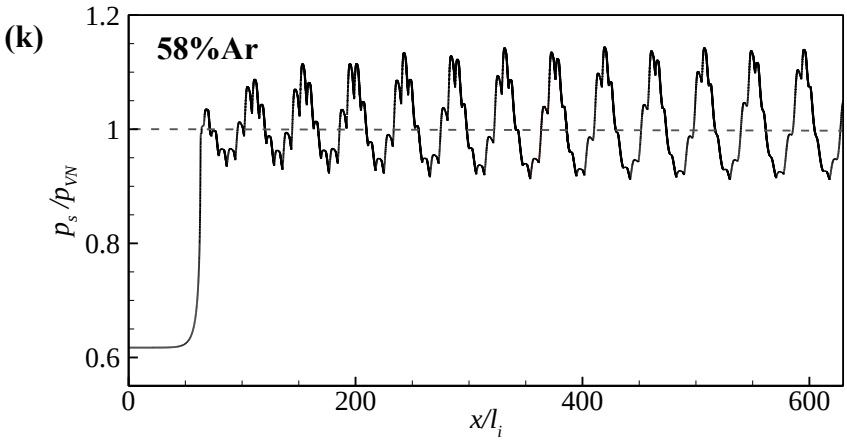
(k)
58%Ar
1.2
1
0.8
0.6
p_s/p_{VN}
0
200
400
600
x/l_i

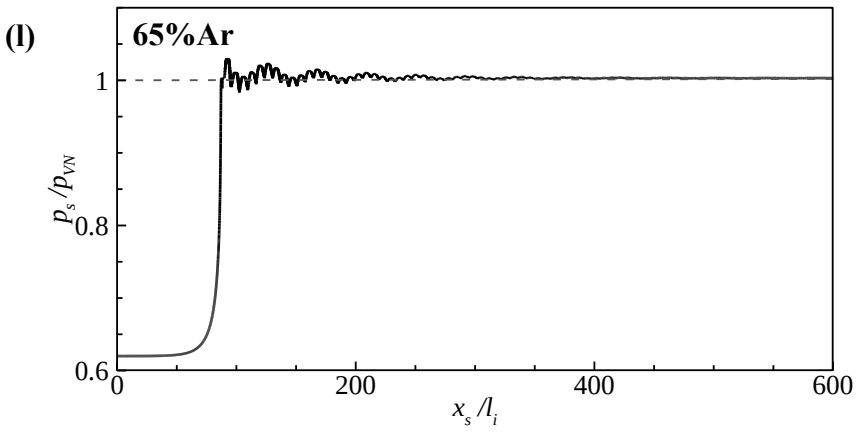
(l)
65%Ar
1
0.8
0.6
p_s/p_{VN}
0
200
400
600
x_s/l_i

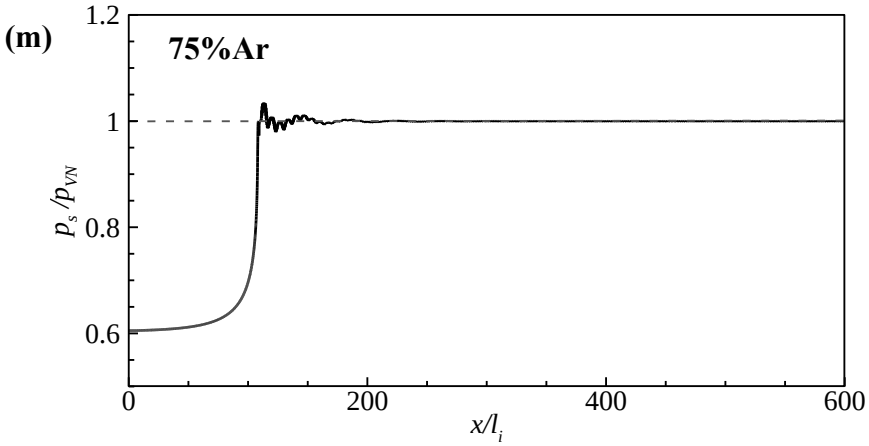
(m)
75%Ar
1.2
1
0.8
0.6
p_s/p_{VN}
0
200
400
600
x/l_i

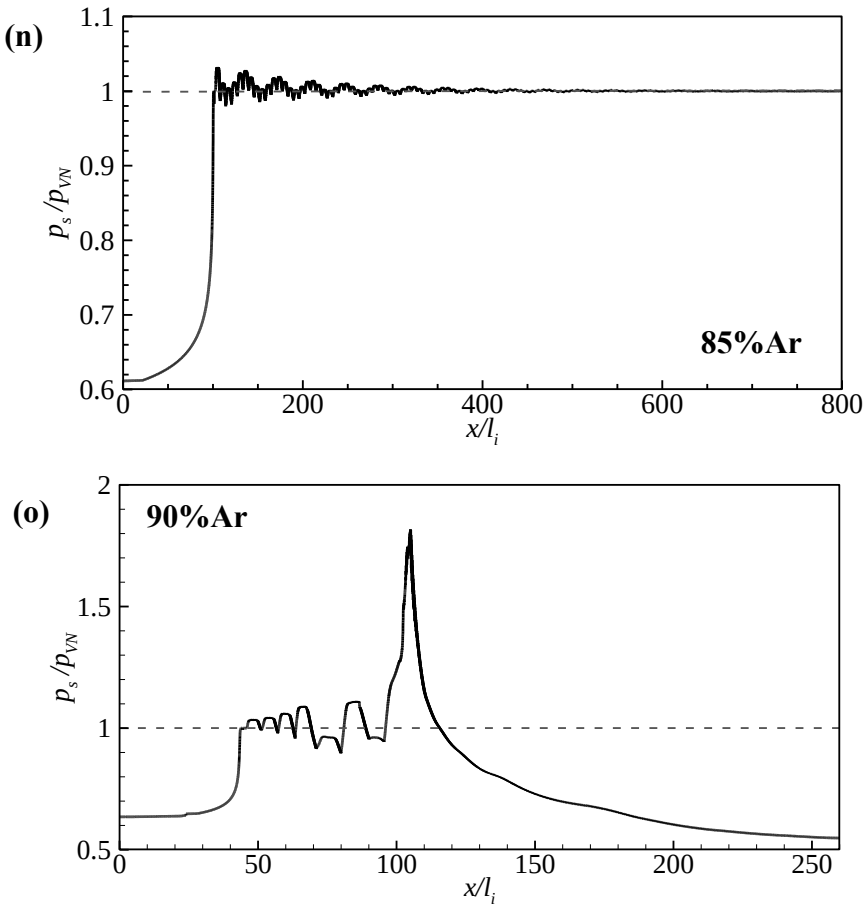

Fig. 4 Maximum pressure histories for different Ar dilutions: The region with low pressure is steady ZND structure as initial condition; the induction length, l_i corresponds to respectively each Ar dilution, and p_{VN} is the steady von-Neumann value corresponding to each case.

Fig. 4 shows that for 15%Ar the detonation fails to sustaining after several high-frequency oscillations, which is substantiated by completely decoupling of the leading shock with the reaction front at x/l_i ~150 shown in Fig. 5(a, b). The reaction zone in detonation structure is rather short and the detonation is highly unstable for 15%Ar dilution. During the phase of decay, bulk unreacted gas escapes from the leading shock and is left behind the front, leading to failure of the propagation. Investigation of the reaction zone structure during the decay revealed that failure occurs due to highly pulsating instability. When the post-shock temperature decays below ~$0.7T_{VN}$, reaction rate is found to be too slow to maintain the coupling with the exothermic part of reaction

zone that is required to drive the wave. As a result, the reaction layer then completely decouples from the shock and the detonation quenches. This failure scenario was previously observed and studied by Short et al. [18,35] in their numerical simulations using a simplified three-step chain-branching reaction scheme. Consequently, for 1-D detonation at a global CJ speed, there is also a limit behavior at 15% Ar dilution because the instability can kill a formed detonation.

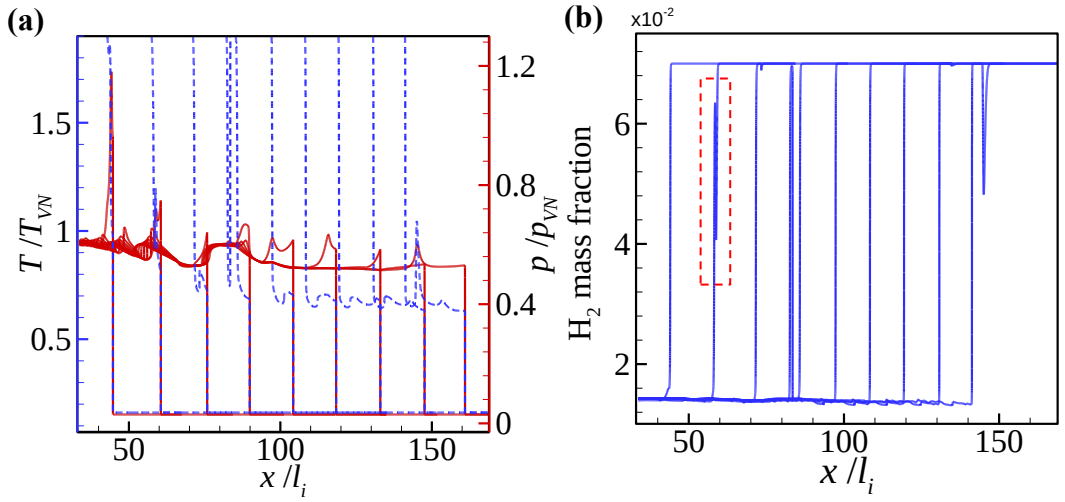

Fig. 5 Frontal structure in process of quenching detonation for 15%Ar dilution: t=0.396, 0.54,0.63, 0.765, 0.899, 1.01, 1.15, 1.29, 1.41μs. T_{VN} is the steady von-Neumann value.

Figure 6 shows the evolution of front structure in decay of the detonation for 90%Ar dilution. It is seen that after several high-frequency oscillations, a strong pulse appears and an overdriven detonation forms, with the peak pressure of ~1.8p_{VN}. After the strong pulse, the overdriven detonation decays significantly and main reaction layer recedes from the leading shock, resulting in long induction zone with a temperature gradient. However, as it decays below C-J state, a fast flame in high-temperature region fails to acceleration and cannot catch up with the leading shock due to low heat release rate led by the large dilution, although it propagates in the temperature gradient. The measured

speed of leading shock wave is ~ 1.2 (964.9m/s), while the speed of reaction front is ~ 0.8 (660.4m/s) at x/l_i ~ 250-350. The shocked temperature and pressure are 939.8K and 9.1atm respectively; and the corresponding autoignition time of gas shocked is so long that reinitiation does not happen. Furthermore, unreacted H_2 fuel shown by H_2 mass fraction in Fig. 6(b) is observed in decay of the overdriven detonation. For 90%Ar, the autoignition time is long and the heat release rate is low due to low shocked temperature and pressure. In this manner, the coupling between the dynamical limit and the autoignition limit will produce the detonability limits.

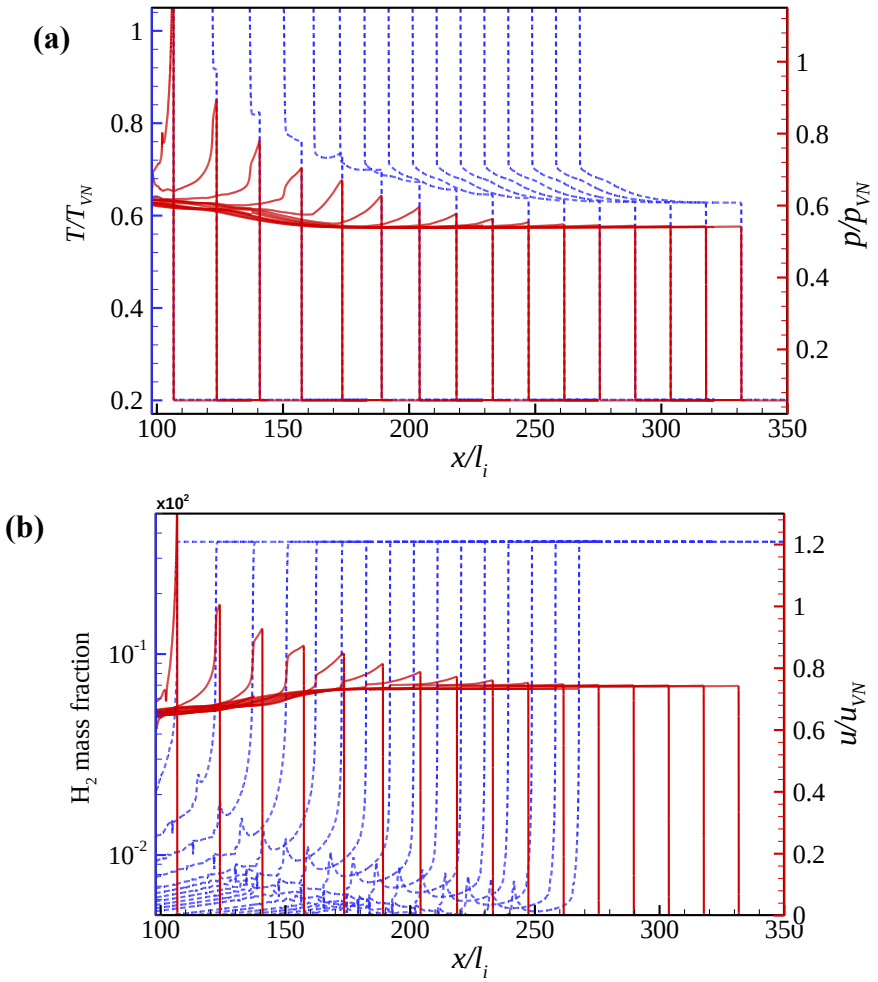

Fig. 6 Frontal structure in process of quenching detonation for 90%Ar dilution: t=67.75, 84.6, 104.11, 124.51, 144.9, 165.3, 185.7, 207.0, 224.7, 245.1, 266.4, 285.9, 305.4, 324.9, 346.2 and 368.4μs.

In summary, three detonation modes, respectively exhibiting stable, periodic, and

chaotic behavior, have been identified with detailed reactions and by varying the mixture composition, similar to those reported by Sharpe & Falle [14] and Ng *et al.* [16]. The instability increases with the thermal sensitivity of distribution of heat release as it is the case when decreasing the dilution. Modification of the ZND structure produced by Ar dilution is the cause of 1-D pulsating instability because the ignition delay time in shocked gas is changed. For 15%Ar dilution, strong instability leads to the failure of a sustaining detonation in 1-D problem, indicating that the detonation is near limit propagation. Furthermore, for the mixture with large dilution of 90%Ar, once the detonation decays to the minimum level where the chemical reaction rate is slow and the induction time is long, a very small quantity of heat release rate may make the re-establishment of detonation impossible. For the 1-D limit Ar dilution, the corresponding 2-D simulation will be presented latter.

Figure 7 shows phase space plots for periodical pulsation with 45%Ar, 48%Ar, 50%Ar and 75%Ar, respectively. It is seen clearly that the four-lobe phase space is exhibited for 45%Ar, while the two-lobe phase space is observed for 48%Ar; the one-lobe phase space presents in the single-period detonation with 50%Ar, while for 75%Ar there is no bounding of shock pressure and the curve gradually rotates to a point (steady shock pressure). It is seen that there are the maximum and minimum dp_s/dt during the compression and expansion phases of one pulsation respectively. During compression phase, dp_s/dt rises and reaches the maximum; while as the pressure is close to the peak, dp_s/dt is equal to zero; during the expansion phase, dp_s/dt is negative and the shocked pressure decreases to the minimum during one pulsation. It is observed that the phase

space plots differ from that with one-step reaction model [1]. This may be because heat release rate for the one-step reaction model is not controlled as real chemistry, with which the induction zone is not distinguished clearly from detonation structure. Consequently, the change rate of shock pressure differs from that with the one-step reaction model, leading to the difference in phase space plots.

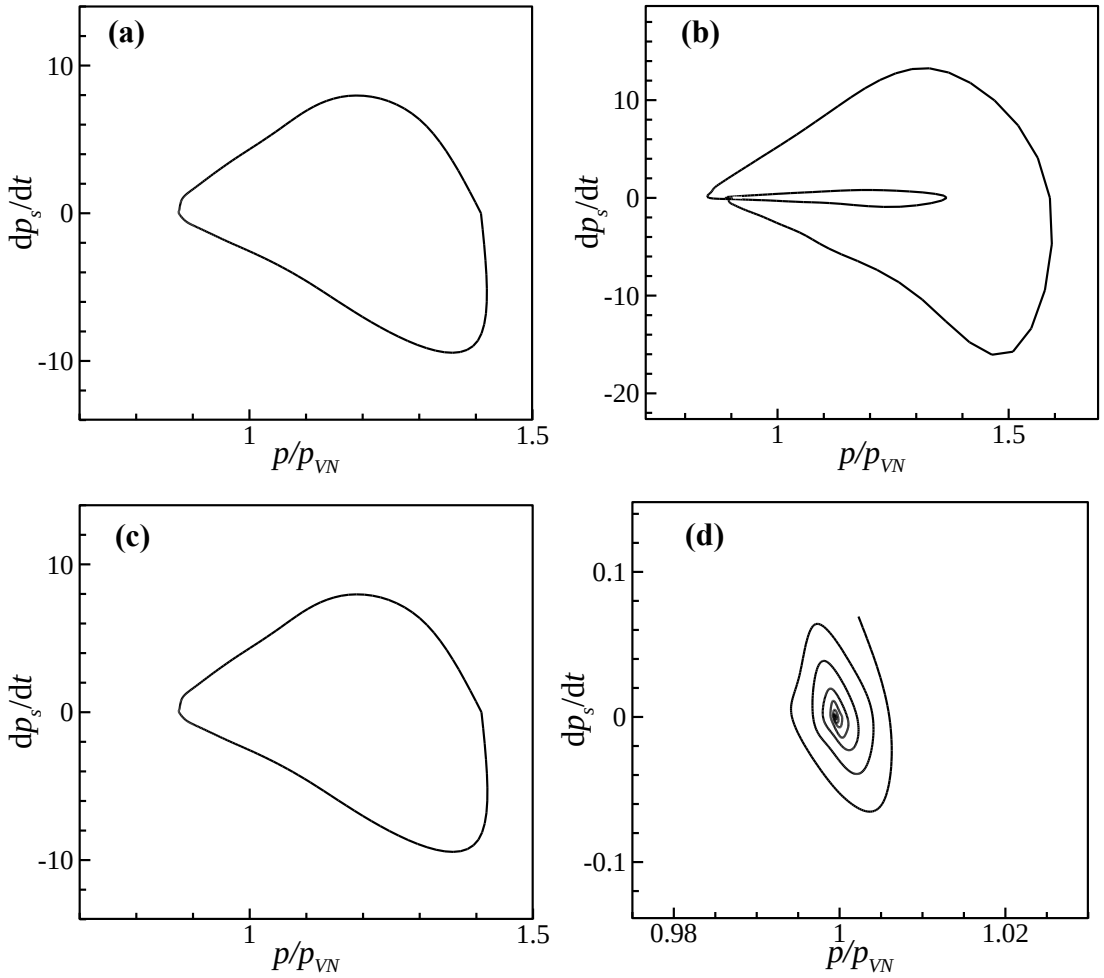

Fig. 7 Phase space plot for different Ar dilutions: (a) 45%Ar, (b) 48%Ar, (c) 50%Ar and (d) 75%Ar.

3.3 Bifurcation of pulsation for different Ar dilutions

He & Lee [30] demonstrated that for other parameters being fixed, there are two critical reduced activation energies to classify planar detonation into stable, unstable

and infinite-large period modes, and pointed out that the numerical simulations with detailed chemistry should be carried out for study of the phenomena observed with a one-step reaction model. The present results with detailed reactions for H_2-O_2-Ar system show bifurcation diagram, as shown in Figs. 8 and 9. The 1-D detonations with real chemistry are classified into three classes. We observe that there exists the critical value between 65% and 50%Ar to transition from the stable to single-period pulsation. The bifurcation point from single-period to period-doubling mode appears between 50% and 48%Ar; see Fig. 8(a). The bifurcation diagram related to the induction length is shown in Fig. 8(b).

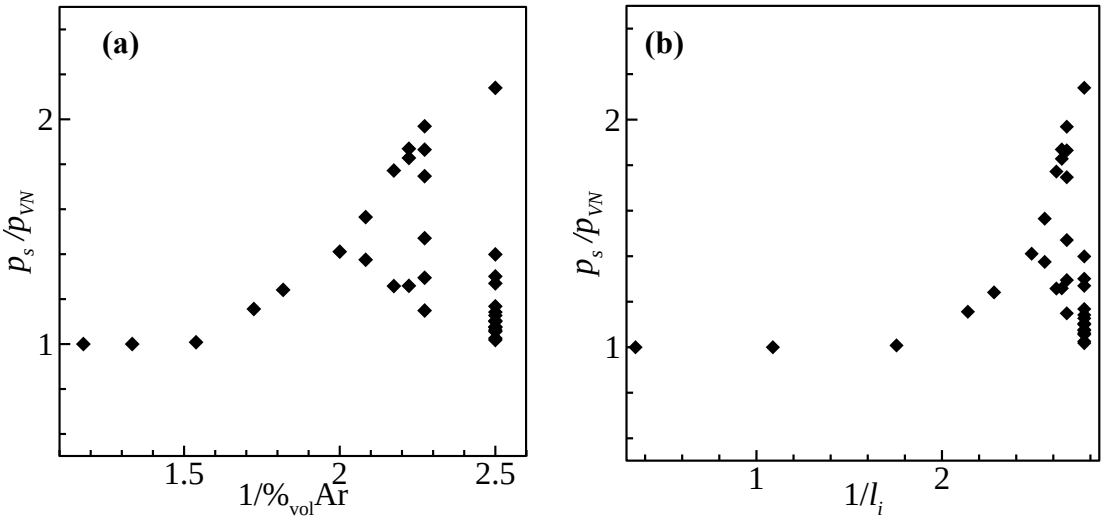

Fig. 8 Bifurcation diagram: peak shock pressure vs. Ar dilution (a) and induction length (b).

For detailed reaction mechanism, the bifurcation diagram with an effective activation energy is shown in Fig. 9. Conventionally, a reduced activation energy, E_a/R_uT_{VN}, can be obtained from an Arrhenius plot of ln(τ) vs. 1/T, characterizing the temperature sensitivity of the induction time. For a one-step reaction model or an elementary reaction with a single activation energy, the result is

$$\ln(\tau) = \frac{E_a}{R_u T} + \text{constant} .$$

For multi-step kinetics, the reduced activation energy, E_a/R_uT_{VN} can be determined by

$$\frac{E_a}{R_u T_{VN}} = \frac{1}{T_{VN}} [\ln(\tau+) - \ln(\tau-)] / (\frac{1}{T+} - \frac{1}{T-}) .$$

Here $T+$ and $T-$ bracket T_{VN}, i.e. $T\pm = T_{VN} \times(1\pm0.01)$, and $\tau+$ and $\tau-$ are the corresponding induction times [31-34]. It is calculated that the stability boundary is between 31.76 and 32.08, and the bifurcation of period-doubling is approximately 32.2 in the present diagram.

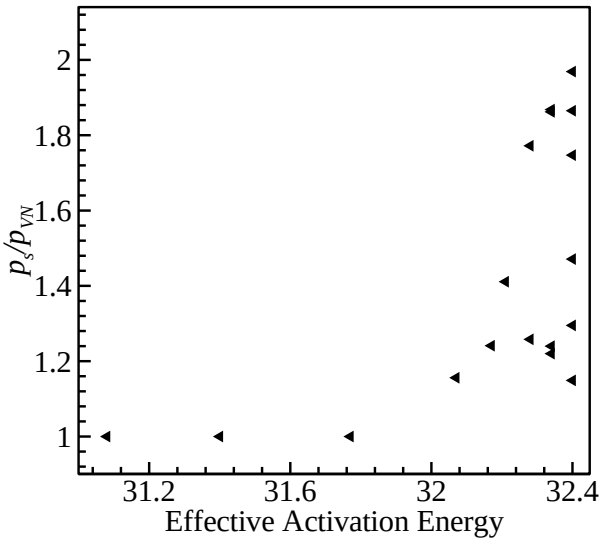

Fig. 9 Bifurcation diagram indicated by shock pressure as a function of effective activation energy.

The curve of stability parameter, $\chi = E_a/RT_{VN} \cdot l_i/l_R$, are shown in Fig. 10. Generally, it is demonstrated that Ng's criterion [16] works on prediction of 1-D detonation instability for H_2-O_2 system with different Ar dilutions.

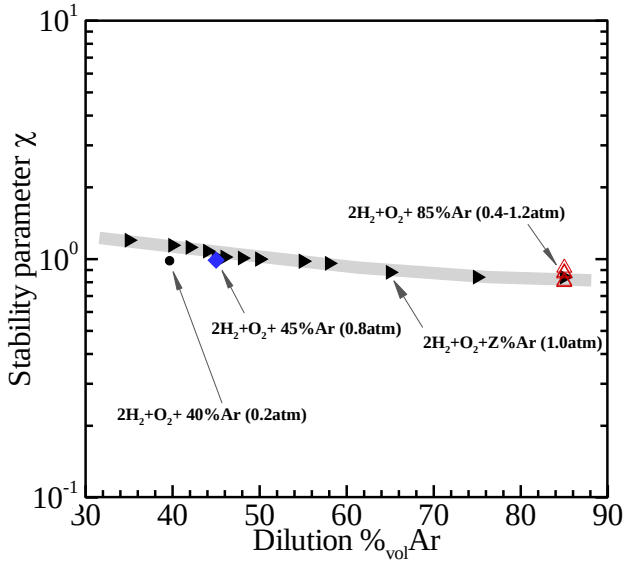

Fig. 10 Stability factor, χ as a function of dilution.

3.4 Detonation limits

From above discussion, it is found the detonability limit at 90% Ar dilution for the propagation starting from a steady 1-D detonation at the globally CJ state. However, if it can be initiated directly by the source energy, a blasting cap even needs to be required for a highly Ar diluted mixture. Therefore, we carry out the simulation of a direct initiation to identify the detonation limit of 90%Ar through an evolution from a strongly source energy (p=10atm, T=2100K in the initiation region). Fig. 11 shows that a strongly overdriven detonation can be produced by a high source energy, and then decays to be CJ state and triggers a strong pulse, demonstrating that a successful initiation can be formed. After undergoing the strong pulse, a formed detonation fails to sustaining. As considering the corresponding 2-D case, eventually the detonation still does not sustain, as substantiated by the maximum pressure in Fig. 11. Consequently, for 90%Ar, failure happens again through a direct initiation from a strong source energy. Furthermore, we study the detonation initiation by setting a temperature gradient to identify whether a detonation eventually quenches. Due to gradient mechanism, a

detonation can be triggered. A strongly overdriven detonation is formed in the region with the temperature gradient. When the detonation goes out the region with gradient, it undergoes a strong pulse and then decays and eventually quenches in the uniform region. This also substantiates that a detonation limit is at 90%Ar dilution.

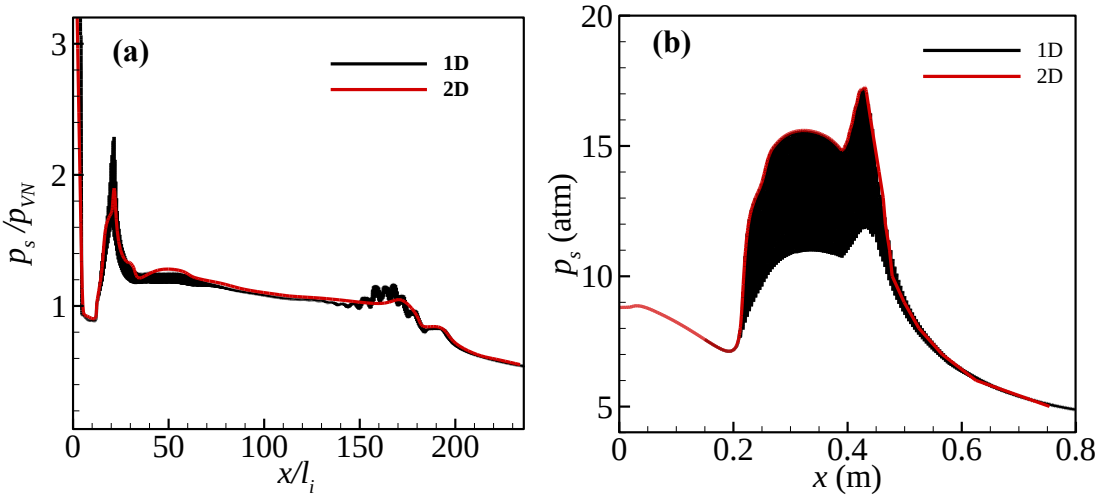

Fig.11 Initiation led by high energy source (a) and induced temperature gradient (b) for 90%Ar. The black shaded region in (b) is caused due to longitudinally and high-frequency oscillation of shock pressure for the 1-D case.

Radulescu *et al*. [18] demonstrated that a highly unstable detonation in 1-D simulation was prone at failure to survive for highly active mixture. The present simulations show that as Ar dilution decreases to 15%Ar, the detonation becomes more unstable and cannot sustain. It is interest to identify whether there is a limit behavior at 15% Ar dilution. Hence, we select 15%Ar dilution to carry out 1-D and 2-D simulations with grid resolution of 1×10^{-6}mm (60pts/$l_{1/2}$), identifying the propagation of 1-D and 2-D detonations produced by a sub-critical direct initiation with T=2100K and p=4atm. For the 1-D case, the detonation wave decays from the initial overdriven to the CJ state and undergoes low-velocity phase. During the low-velocity phase, the leading shock decays. Although the leading shock decays below approximately $0.8p_{VN}$, it can reinitiate

unreacted gas to form a detonation, with a pressure pulse at x/l_i ~70; subsequently it decays again below ~0.6 p_{VN} at x/l_i ~140 and quenches eventually. This demonstrates that the 1-D initiation fails by the sub-critical way; see black line in Fig. 12(a). However, as considering 2-D instability, a cellular detonation appears at x/l_i ~50 and sustains, with irregular cells shown in Fig. 12(b). Consequently, the initiation fails in the 1-D simulation, while it succeeds in the 2-D case, demonstrating that cellular instability is beneficial for sustaining a detonation in the confinement domain.

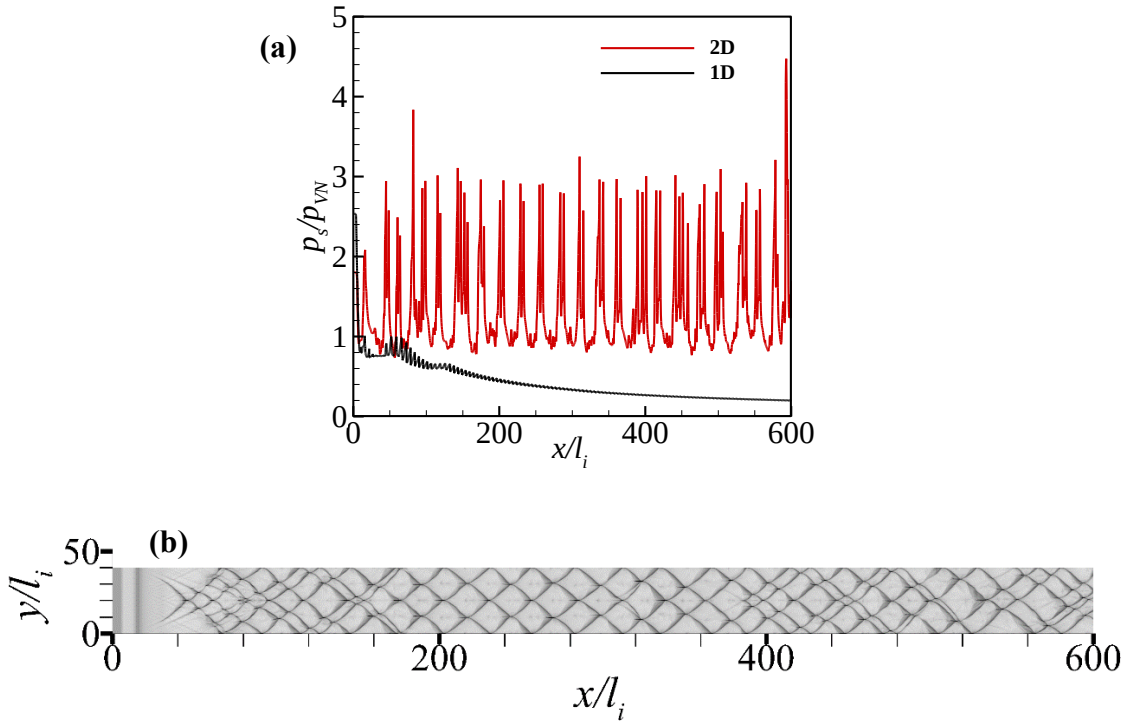

Fig. 12 1-D and 2-D initiation by a sub-critical way for 15%Ar dilution: red line is maximum pressure histories along the center of 2-D domain in (a); cellular feature in (b).

In summary, using the realistic chemical kinetic model for H_2-O_2 mixtures, the present numerical results indicate that for 15%Ar dilution, the 1-D pulsating detonation cannot sustain due to high instability, while the 2-D cellular detonation can sustain. In the 1-D detonation, ignition can only be achieved via adiabatic shock induction. Therefore, there are no other mechanisms to effect ignition. However, in multi-dimensional

detonations, ignition behind the strong transverse shocks, by transverse wave interactions and turbulent mixing, can provide alternate means to effect autoignition and thus maintain the detonation propagation. The role of transverse waves thus becomes essential to sustain the detonation propagation for highly unstable detonations [36, 37]. For 15%Ar dilution, transverse waves play important role in self-sustaining propagation in the confined domain; the detonation always fails when transverse waves are eliminated [37]. In unconfined space, as role of transverse waves weakens and the re-amplification of transverse waves disappears, it is more difficult to sustain a cellular detonation [38].

4. Conclusions

The structure and propagation of one-dimensional (1-D) detonations is investigated by high-resolution simulation for the H_2-O_2 system with different Ar dilutions. Three detonation modes are observed, namely the highly unstable, chaotic detonation, the mildly unstable detonation with either multi- and single-period pulsations, and the stable detonation. As Ar dilution increases, detonatinity limit is found, which is led by low heat release rate due to dilution effect. The bifurcation diagram of 1-D detonation instability is established and global bifurcation diagram is similar to that by the 1-step model. Eventually, the numerical results demonstrate that for real chemistry, the criterion of Ng. et al. [16] still works well on prediction of 1-D detonation instability. Ng et al. [16] studied the pulsating instability of 1-D detonation for different reaction parameters in a two-step simplified model, and established a bifurcation diagram as a parameter controlling a reaction time in the model. It is of

interest to compare the present results with the two-step and three step models in future work.

Acknowledgements

This research is supported by the National Natural Science Foundation of China under grants 11972090 and 11732003, and Science and Technology on Transient Impact Laboratory Foundation (Grant No. 6142606182104). The research is also supported by the European Commission for the Marie Curie International Fellowships Grant "TurbDDT (Grant No. 793072)".

References:

[1] J.H.S. Lee, The Detonation phenomena, Cambridge University Press, Cambridge, New York, 2008.

[2] P. Clavin, L.T. He, Stability and nonlinear dynamics of one dimensional overdriven detonations in gases, J. Fluid Mech. 306(1996) 353-378.

[3] P. Clavin, B. Denet, Diamond patterns in cellular fronts of overdriven detonation, Phys. Rev. Lett. 88(2002) 044502.

[4] P. Clavin, L. He, F.A. Williams, Multidimensional stability analysis of overdriven gaseous detonations, Phys. Fluids 9(1997) 3764-3785.

[5] G. Lodato, L.Vervisch, P. Clavin, Direct numerical simulation of shock wavy-wall interaction: analysis of cellular shock structure and flow patterns, J. Fluid Mech. 789(2016) 221-258

[6] J.B. McVey, T.Y. Toong, Mechanism of instabilities of exothermic hypersonic blunt body flows, Combust. Sci. Tech. 3(1971) 63-76.

[7] A. Matsuo, K. Fujii, T. Fujiwara, Flow features of shock-induced combustion around projectile traveling at hypervelocities, AIAA J. 33(1995) 1056-1063.

[8] H.I. Lee, D.S. Stewart, Calculation of linear detonation instability-one-dimensional instability of plane detonation, J. Fluid Mech. 216(1990) 103-132.

[9] M. Short, A.K. Kapila, J.J. Quirk, The chemical-gas dynamic mechanisms of pulsating detonation wave instability, Phil. Trans. R. Soc. Lond. A 357(1999) 3621-3637.

[10] M. Short, G.J. Sharpe, Pulsating instability of detonations with a two-step chain-branching reaction model: Theory and numerics, Combust. Theor. Model. 7(2003) 401-416.

[11] C. Leung, M.I. Radulescu, G.J. Sharpe, Characteristics analysis of the one-dimensional pulsating dynamics of chain-branching detonations, Phys. Fluids 22 (2010) 126101.

[12] P. Clavin, F.A. Williams, Dynamics of planar gaseous detonations near Chapman-Jouguet conditions for small heat release, Combust. Theor. Model. 6 (2002) 127

[13] L. He, J. H. S. Lee, The dynamical limit of one-dimensional detonations, Phys. Fluids 7(1995) 1151-1158.

[14] G.J. Sharpe, S.A.E.G. Falle, One-dimensional numerical simulations of idealized detonations, Proc. R. Soc. Lon. 455(1999) 1203-1214.

[15] C.M. Romick, T.D. Aslam, J.M. Powers, The effect of diffusion on the dynamics of unsteady detonations, J. Fluid Mech. 699(2012)453-464.

[16] H.D. Ng , M.I. Radulescu, A.J. Higgins, N. Nikiforakis, J.H.S. Lee, Numerical investigation of the instability for one-dimensional Chapman-Jouguet detonations with chain-branching kinetics, Combust. Theor. Model. 9 (2005) 385-401.

[17] M. Short, J.J. Quirk, On the nonlinear stability and detonability limit of a detonation wave for a model three-step chain-branching reaction, J. Fluid Mech. 339 (1997) 89-119.

[18] M.I. Radulescu, H.D. Ng, J.H.S. Lee, B. Varatharajan, The effect of argon dilution on the stability of acetylene-oxygen detonations. Proc. Combust. Inst. 29(2002) 2825-2831.

[19] S. Yungster, K. Radhakrishan, Pulsating one-dimensional detonations in hydrogen-air mixtures. Combust. Theor. Model. 8 (2004) 745-770

[20] C.M. Romick, T.D. Aslam, J.M. Powers, Verified and validated calculation of unsteady dynamics of viscous hydrogen-air detonations. J. Fluid Mech., 769(2015) 154-181.

[21] J.M. Powers, S. Paolucci, Accurate spatial resolution estimates for reactive supersonic flow with detailed chemistry, AIAA J. 43 (2005)1088-1099.

[22] J.L. Ziegler, R. Deiterding, J.E. Shepherd, D. I. Pullin, An adaptive high-order hybrid scheme for compressive, viscous flows with detailed chemistry, J. Comput. Phys. 230 (2011) 7598-7630.

[23] M.A. Sussman, Numerical simulation of shock-induced combustion, PhD thesis, Stanford University, 1995.

[24] R.J. Kee, F.M. Rupley, J.A. Miller, Chemkin II: a Fortran chemical kinetics package for the analysis of gas phase chemical kinetics. Tech. Rep. SAND89-8009B. Sandia National Laboratories. 1992

[25] R. J. Kee, G. Dixon-Lewis, J. Warnatz, M.E. Coltrin, J.A. Miller, A Fortran computer code package for the evaluation of gas-phase multi-component transport properties. Tech. Rep. SAND86-8246. Sandia National Laboratories. 1991.

[26] A.L. Sánchez, F.A. Williams, Recent advances in understanding of flammability characteristics of hydrogen, Prog. Energ. Combust. 41 (2014) 1-55.

[27] G.S. Jiang, C.W. Shu, Efficient implementation of weighted ENO schemes, J. Comput. Phys. 126 (1996) 202-228.

[28] C.A. Kennedy, M.H. Carpenter, Additive Runge-Kutta schemes for convection diffusion reaction equations, Appl. Numer. Math. 44(2003) 139-181.

[29] C. Wang, C.W. Shu, W.H. Han, J.G. Ning, High resolution WENO simulation of 3D detonation waves, Combust. Flame 160 (2013) 447-462.

[30] H.D. Ng, A.J. Higgins, C.B. Kiyanda, M.I. Radulescu, J.H.S. Lee, K.R. Bates, N. Nikiforakis, Nonlinear dynamics and chaos analysis of one-dimensional pulsating detonations, Combust. Theor. Model. 9 (2005) 159-170.

[31] L.T. He, J.H.S. Lee, The dynamical limit of one-dimensional detonations. Phys. Fluids 7 (1995) 1151.

[32] J.M. Austin, F. Pintgen, J.E. Shepherd, Reaction zones in highly unstable detonations. Proc. Combust. Inst. 30 (2005) 1849-1857.

[33] F. Pintgen, J.E. Shepherd. Pulse detonation engine impulse analysis for partially-oxidized jet fuel. GALCIT Report FM2003.001, 2003. 5.

[34] E. Schultz, J.E. Shepherd, Validation of detailed reaction mechanisms for detonation simulation, Technical Report FM99-5, GALCIT, 2000. 5.

[35] M. Short, J.J. Quirk, On the nonlinear stability and detonability limit of a detonation wave for a model three-step chain-branching reaction. J. Fluid Mech. 339 (1997) 89-119.

[36] A. Teodorczyk, J.H.S. Lee, Detonation attenuation by foams and wire meshes lining the walls. Shock Waves 4 (1995)225-236.

[37] M.I. Radulescu, The failure and initiation mechanism of detonations propagating in porous wall tubes, Ph.D. dissertation, McGill University, Montreal, Quebec, 2002.

[38] W.H. Han, C. Wang, C.K. Law. Pulsation in one-dimensional H2-O2 detonation with detailed reaction mechanism. Combust. Flame 200 (2019) 242-261.